Possible observation of quantum spin-nematic phase in a frustrated magnet

Yoshimitsu Kohama[a,1], Hajime Ishikawa[a], Akira Matsuo[a], Koichi Kindo[a], Nic Shannon[b,c], and Zenji Hiroi[a]

[a]Institute for Solid State Physics, University of Tokyo, Kashiwa, 277-8581 Chiba, Japan; [b]Theory of Quantum Matter Unit, Okinawa Institute of Science and Technology Graduate University, Onna-son, 904-0412 Okinawa, Japan; and [c]Department of Physics, Technical University of Munich, 85748 Garching, Germany

Edited by Robert J. Cava, Princeton University, Princeton, NJ, and approved April 16, 2019 (received for review December 25, 2018)

Water freezes into ice in winter and evaporates into vapor in summer. Scientifically, the transformations between solid, liquid, and gas are called phase transitions and can be classified through the changes in symmetry which occur in each case. A fourth phase of matter was discovered late in the 19th century: the liquid crystal nematic, in which rod- or disk-shaped molecules align like the atoms in a solid, while continuing to flow like a liquid. Here we report thermodynamic evidence of a quantum analog of the classical nematic phase, the quantum spin nematic (SN). In an SN, the spins of a quantum magnet select a common axis, like a nematic liquid crystal, while escaping conventional magnetic order. Our state-of-the-art thermal measurements in high pulsed magnetic fields up to 33 T on the copper mineral volborthite with spin 1/2 on a frustrated lattice provide thermodynamic evidence for SN order, half a century after the theoretical proposal [Blume M, Hsieh YY (1969) *J Appl Phys* 40:1249; Andreev AF, Grishchuk IA (1984) *J Exp Theor Phys* 97:467–475].

magnetism | high magnetic field | hidden order | spin nematic | calorimetry

The historical discovery of liquid crystals demonstrated the existence of a new state of matter beyond solid, liquid, and gas. Once a scientific curiosity, liquid crystals now form the basis for a wide range of technologies, including the majority of electronic displays. The identification of a spin nematic (SN) would be a significant achievement as it represents a new quantum phase of matter, with qualitatively different properties from any known phase in a magnet. Moreover, SNs also have considerable potential for application, notably in magnetic refrigeration and quantum computation. However, searching for SNs in experiments is very challenging because it is a form of "hidden order" (1), a term used to describe thermodynamic phase transitions where the changes in symmetry are unknown or very hard to detect.

There is good theoretical evidence that SN order should occur in a wide range of systems, including thin films of ^{3}He; cold atoms in an optical lattice; and a wide variety of quantum magnets with competing, or "frustrated," interactions. The simplest candidate is the spin-1 system in which spin quadrupole moments of spin-1 form a quadrupolar order (2), although its observation is still elusive (3). Among other widely discussed examples are quantum spin chains (4–8) and square-lattice Heisenberg models (9–12) where ferromagnetic first-neighbor interactions (J_1) compete with antiferromagnetic second-neighbor interactions (J_2), in applied magnetic field. In these systems, the magnon excitations of the high-field saturated state form a bound pair on the bond of J_1 (effective spin-1 state), which then undergo Bose–Einstein condensation (BEC), much like bound pairs of electrons in a superconductor (7, 13) (Fig. 1). Since each bound pair of magnons carries a quadrupole moment (Fig. 2*B*), the resulting BEC is an SN, characterized by an ordered arrangement of quadrupole moments on first-neighbor bonds, which mimic the rod- or disk-like molecules in the liquid crystal nematic (12) (Fig. 2*C*). The observation of an SN in experiment would be very significant since, while single-particle BECs have been observed in magnets (14), the SN would represent the first example of a pair condensate. However, the quadrupole moments in SNs do not break time-reversal symmetry (2), and so they cannot be detected using the common probes of magnetic order (12), rendering the SN a hidden-order phase.

SN order has been discussed in a number of materials, with candidates including $LiCuVO_4$ and $NaCuMoO_4(OH)$, as realizations of a frustrated ferromagnetic spin chain (15–17), and $Ba_2CdVO(PO_4)_2$ as an example of a square-lattice frustrated ferromagnet (18). To date, however, conclusive experimental evidence for an SN remains elusive. At present, the best-documented system is $LiCuVO_4$, where a recent low-temperature NMR study identified a narrow range of magnetic field, approaching saturation, for which the local magnetization remains homogeneous and uniform, while its value is field dependent (16). This behavior is consistent with a SN state, but evidence for a corresponding thermodynamic phase transition is lacking.

Volborthite [$Cu_3V_2O_7(OH)_2{\cdot}2H_2O$], a mineral named after the Russian paleontologist Alexander von Volborth, is one of the most exotic quantum magnets in nature. First suggested as an example of a kagome antiferromagnet (Fig. 2*A*), volborthite is now considered to be a square-lattice frustrated ferromagnet (19), in which groups of three Cu atoms (trimers) combine to form spin-1/2 moments on a distorted square lattice, coupled by competing ferromagnetic (J_1) and antiferromagnetic (J_2 and J_2') exchange interactions (cf. Fig. 2*B*). Theoretical estimates place volborthite in a parameter range for which two-magnon bound states have a tendency to condense (19), leading to SN order (9). On the experimental side, measurements of magnetization, shown in Fig.

Significance

Spin-nematic state in frustrated ferromagnet is one of the exotic states of matter at high magnetic field that could arise as the Bose–Einstein condensation of the two-magnon bound state. Its experimental detection in a real material has long been hindered by the fact that the order parameter of the spin-nematic state, spin quadrupole moment, is hard to detect with conventional magnetic probes available in high magnetic field. Here we design a calorimeter for the pulsed magnetic field studies and perform state-of-the-art measurements of heat capacity and magnetocaloric effect up to 33 T. These results provide strong prima facie evidence for a spin-nematic state in the copper-based mineral volborthite.

Author contributions: Z.H. designed research; Y.K., H.I., A.M., and K.K. performed experiments; Y.K., N.S., and Z.H. analyzed data; and Y.K., N.S., and Z.H. wrote the paper.

The authors declare no conflict of interest.

This article is a PNAS Direct Submission.

[1]To whom correspondence should be addressed. Email: ykohama@issp.u-tokyo.ac.jp.

This article contains supporting information online at www.pnas.org/lookup/suppl/doi:10.1073/pnas.1821969116/-/DCSupplemental.

Published online May 9, 2019.

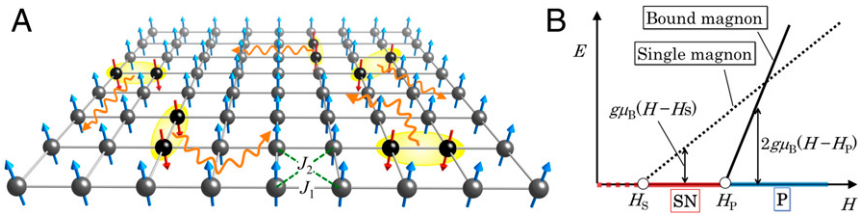

Fig. 1. SN state expected for a square-lattice frustrated ferromagnet in applied magnetic field. (*A*) Schematic picture of bound pairs of magnons moving in a background of field-polarized spins, following ref. 13. Magnetic moments (spins) interact through competing ferromagnetic first-neighbor (J_1) and antiferromagnetic second-neighbor interactions (J_2). Here the majority of magnetic ions (gray spheres) have moments aligned with an external magnetic field (blue arrows). Flipped spins (red arrows) gain energy by propagating as bound pairs. (*B*) Energy of one- and two-magnon excitations, relative to the field-polarized state (P), as a function of magnetic field (H). The SN state is formed through the condensation of bound pairs of magnons (9–11). This occurs when the magnetic field falls below a critical field determined by the two-magnon binding energy (H_P). SN order occurs when H_P is greater than the critical field for condensation of a single magnon (H_S).

2C, reveal a smoothly increasing magnetization, terminating in a broad magnetization plateau, P at $H_P = 27.5$ T. The value of the magnetization within this plateau is consistent with 1/3 of the spins being aligned with the magnetic field, as expected for trimers with a net spin-1/2 moment.

Parallel NMR experiments (20, 21) provide valuable information about magnetic correlations. Within the magnetization plateau, ^{51}V NMR presents a single sharp line, consistent with a uniform distribution of internals fields, at an energy independent of magnetic field. Meanwhile, for $4.5 < H < 22.5$ T (phase II in Fig. 2C), NMR reveals a broad distribution of internal fields, bounded by two distinct peaks, characteristic of a spin-density wave (SDW) state. For intermediate fields $22.5 < H < 27.5$ T, magnetization increases sharply, and the ^{51}V NMR line undergoes a complex evolution, which is not consistent with either an SDW or conventional magnetic order. This evolution can be divided into two regimes, one from $22.5 < H \leq 25$ T, where two peaks are resolved, and a second from $25 < H < 27.5$ T, where the NMR line shape shows the same structure as in the 1/3 plateau, with a single sharp peak. In this sense, the situation closely parallels that in $LiCuVO_4$, where the NMR line shape in the proposed SN phase resembles that in the saturated state, and the combination of magnetization, NMR, and theoretical prediction together build a strong case for SN order (16). The remaining challenge, in both cases, is to find clear thermodynamic evidence for a new phase.

To get insight on the possible SN order in volborthite, we have carried out heat capacity (C) and magnetocaloric effect (MCE) measurements under pulsed magnetic fields up to 33 T. These thermodynamic quantities relate to entropy and are sensitive to any phase transition irrespective of the type of order parameter (22). A good demonstration is found for the hidden order of URu_2Si_2, which can be clearly detected by heat capacity and MCE, whereas most other techniques fail (23). However, measuring heat capacity for magnetic compounds under a pulsed magnetic field varying in a short time duration of milliseconds is challenging because the field variation causes temperature

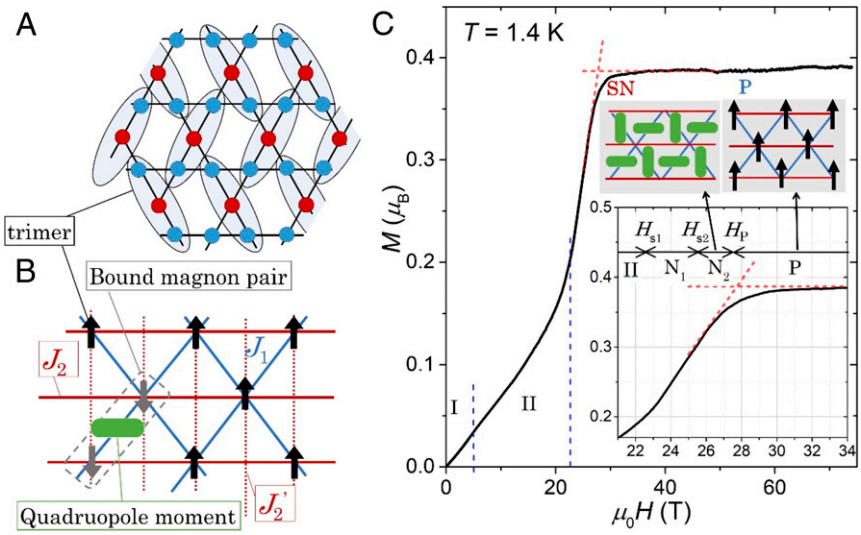

Fig. 2. Microscopic model and experimental magnetization curve of volborthite. (*A*) Spin-1/2 Cu^{2+} ions within volborthite (red and blue disks) occupy the sites of a kagome lattice with highly anisotropic exchange interactions. These moments form trimers, which act as a single effective spin-1/2 moment, with trimers centered on a regular array of lattice sites (red circles). (*B*) The network of trimers within volborthite forms a square lattice of effective spin-1/2 moments (black arrows), with competing ferromagnetic first-neighbor interactions (J_1) and antiferromagnetic second-neighbor interactions J_2, and J_2'. (*C*) Magnetization curve of volborthite, measured at 1.4 K, in pulsed fields of up to 75 T (20). At a critical field of 27.5 T, the magnetization of the spin-1/2 trimers saturates, giving rise to a broad plateau in magnetization. (*Inset*) Detail of magnetization for $H \sim 30$ T, showing the onset of the magnetization plateau. This can be viewed as a polarized state (P) of spins on a square lattice. The condensation of bound pairs of magnons would lead to the formation of a SN with quadrupole moments on first-neighbor bonds (green lozenges). The thermodynamic measurements reported in this article make it possible to distinguish two distinct phases approaching the magnetization plateau, here labeled N_1 and N_2; we identify phase N_2 as an SN. At lower values of magnetic field, volborthite exhibits phase transitions into an incommensurate SDW (II) and an unidentified low-field phase (I).

fluctuation owing to MCE. We have developed a state-of-the-art technique to generate a modified pulsed magnetic field with its top truncated to become almost flat with a high field stability of ±0.01 T, which allows us to measure heat capacity precisely at the flat-top field down to 0.8 K.

We first discuss the phase boundaries found using MCE measurements and then use corresponding result for heat capacity to characterize each of the phases found. Fig. 3*A* shows the evolution of curves of constant entropy, $T(H)_S$, taken from MCE measurements performed under quasi-adiabatic conditions (A-MCE), starting from the state found for $H = 0$ at a given temperature. In all cases the adiabat $T(H)_S$ initially decreases with increasing field, before passing through a broad minimum at $H \sim 25$ T and then increasing, behavior consistent with a phase transition at low temperatures (22). Adiabats become tightly bunched at low temperatures, approaching the onset of the 1/3-magnetization plateau P at $H_P \sim 27.5$ T, suggesting a dense set of low-energy excitations (22). A notable change occurs when the temperature falls below ~1.7 K; the broad minimum in $T(H)_S$ acquires small dips, indicative of phase transitions, at $H_{s1} \sim 22.5$ T and $H_{s2} \sim 25.5$ T and $H_P \sim 27.5$ T. Each of these three critical fields is singled out by a corresponding anomaly in measurements of MCE under approximately isothermal conditions (I-MCE) of $T = 1.25$, 1.0, and 0.75 K (Fig. 3*B*) and the related changes in entropy (Fig. 3*C*). Together with measurements of heat capacity, discussed below, these results clearly delineate two domes in the (H,T) plane, each corresponding to a different low-temperature phase. We label these phases N_1 and N_2 in Fig. 3; N_1 corresponds to the phase N found in earlier NMR experiments (20, 21), and N_2 fills the gap between N and P.

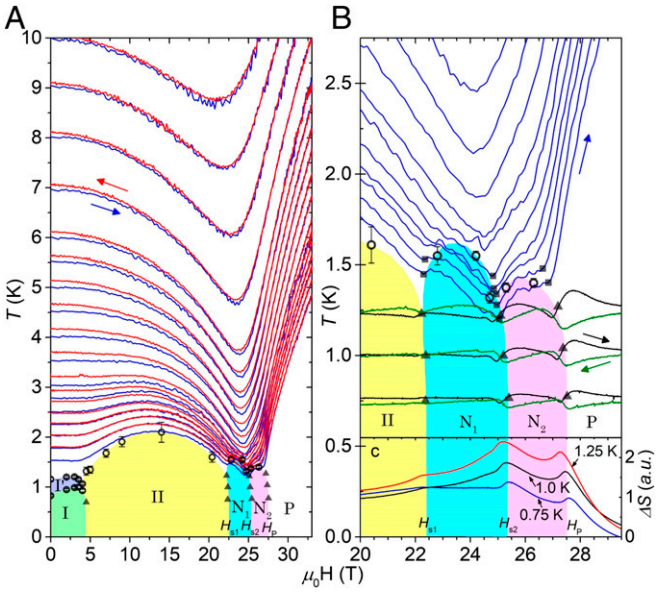

Fig. 3. Magnetocaloric effect and magnetic phase diagram of volborthite. (*A*) Experimental measurements of the MCE in volborthite, showing the evolution of temperature with changing magnetic field under (quasi-)adiabatic conditions (A-MCE). Results are shown for both rising (blue curves) and falling (red curves) magnetic field and reflect contours of constant entropy. The onset of the hidden-order phases, N_1 and N_2, is associated with tight bunching curves and a dip in the entropy contour, corresponding to a change in sign of the MCE. Black triangles show phase boundaries at low temperature, extracted from complimentary measurements of MCE under isothermal conditions (I-MCE). The phase boundaries extracted from measurements of heat capacity, $C(T)$, are shown with open circles. (*B*) Detail of phases N_1 and N_2, showing results for A-MCE measured in rising field (blue curves), I-MCE in rising field (black curves), and I-MCE in falling field (green curves). The black squares show the evolution of a corresponding feature in the A-MCE. Two distinct domes can be resolved at finite temperature, bounded by the critical fields $H_{s1} = 22.5$ T, $H_{s2} = 25.5$ T, and $H_P = 27.5$ T. (*C*) Changes of entropy extracted from measurements of I-MCE at low temperature (*Methods*). The field boundaries of the SN phase, N_2, and presumed supersolid phase, N_1, are sharply distinguished by local anomalies in entropy.

We now turn to measurements of heat capacity, which provide more insight into the nature of the phases N_1 and N_2. Fig. 4 shows the temperature dependence of heat capacity for magnetic field ranging from 0 to 30.2 T. In the absence of magnetic field, $C(T)$ exhibits small peaks at 0.8 and 1.2 K, as reported previously (24) (Fig. 4*A*). The onset of SDW order (II) at intermediate values of magnetic field is revealed in broad shoulders in $C(T)$; these occur at $T \sim 2$ K for $H = 14$ T and $T \sim 1.5$ K for $H = 20.4$ T (Fig. 4*A*), in agreement with phase boundaries found in NMR (24). Very different behavior is observed for $H > H_{s1}$; the transition into the phase N_1 is marked by a substantial λ-shaped anomaly, occurring at $T \sim 1.54$ K for $H = 22.8$ T, in agreement with the phase boundary identified in MCE (Fig. 3). This feature becomes still more pronounced with increasing field (Fig. 4*A*). Meanwhile, the onset of the phase N_2 is accompanied by an extremely sharp peak, consistent with a logarithmic divergence in $C(T)$ (Fig. 4*B*). The crossover into the saturated state, for $H > H_P$, is not accompanied by any anomaly in $C(T)$ (Fig. 4*B*). These results provide unequivocal evidence that N_1 and N_2 are bulk, thermodynamic phases; we find corresponding changes in entropy of $\Delta S = 0.12R\ln 2$ entering phase N_1 at $H = 24.2$ T and $\Delta S = 0.09R\ln 2$ entering phase N_2 at $H = 26.3$ T.

Spontaneous symmetry breaking can produce a gapless Goldstone excitation that gives power-law behavior in the low-temperature heat capacity. For most ordered states including SDW and SN states, one would expect linearly dispersing Goldstone modes (8, 12, 25). These usually contribute to the low-temperature heat capacity as $C(T) \propto T^d$, where d is the spatial dimension of the system. As shown in the log–log plots of Fig. 4 *C* and *D*, the low-temperature heat capacities for phases I and II tend to be proportional to T^3, while for phases N_1 and N_2, $C(T) \propto T^2$. This implies that the character of magnetic excitations changes from 3D to 2D, although it is preferable to increase the temperature range of the fit (*SI Appendix*). Probably, for phases I and II, 3D antiferromagnetic magnons or phasons occur (8) owing to non-negligible interlayer couplings, while the dimensionality of magnetic excitations for phases N_1 and N_2 is qualitatively reduced in the measurement temperature range. This type of dimensional reduction is not surprising in a quasi-2D magnet with SN order, since the opening of a gap to transverse spin excitations will lead to a suppression of interplane exchange.

In the state P, for $H > H_P$, there is no phase transition above 0.8 K, and the low-temperature heat capacity shows exponentially activated behavior (Fig. 4*E*): the 30.2 T data are well described by the equation, $C = \exp[-\Delta/k_BT]/T$ (26), with an activation energy $\Delta = 6.7$ K. We interpret this as a gap to two-magnon excitations, as illustrated in Fig. 1*B* (19). Assuming that this gap opens at $H_P = 27.5$ T and modeling it as $\Delta = g\mu_B(H - H_P)$, we arrive at an effective Landé g factor of $g = 3.7$. It should be noted that the critical field deduced from the phase boundary, H_P^{PB}, lies in the range 27.5–28.0 T, which yields $g = 3.7$–4.5 (*SI Appendix*). These values are nearly twice as large as the single-electron g factor found in electron spin resonance measurements at lower values of field [$g_c = 2.04$ below 12 T (27)], consistent with a two-magnon excitation. The g factor estimated from NMR measurements on volborthite also shows an enhancement to $g \sim 4.6$–5.9 (24), providing further evidence for two-magnon bound states.

To recap, it has been suggested (19) that for a narrow range of H just below H_P, bound pairs of magnons undergo a low-temperature BEC, leading to an antiferroquadrupolar SN order, as illustrated in Fig. 2*C*. At present the case for this SN order rests on a combination of theoretical analysis of the crystal structure and associated magnetic model (19) and NMR experiments which,

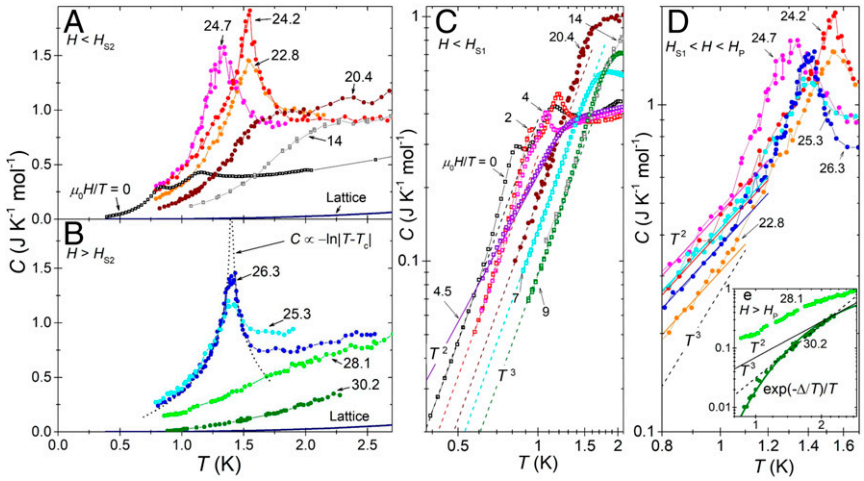

Fig. 4. Heat capacity and thermodynamic evidence for low-energy excitations volborthite. (*A*) Experimental results for heat capacity $C(T)$, for magnetic fields spanning the low-field phase I, SDW phase II, and phase N_1. The onset of N_1 is distinguished by a sharp anomaly in $C(T)$ for $T \sim 1.5$ K. (*B*) Heat capacity within the hidden-order phase N_2 and magnetization plateau P. The onset of N_2 is distinguished by a sharp peak in $C(T)$ for $T \sim 1.4$ K. The form of this peak is consistent with the logarithmic divergence expected for an Ising phase transition in 2D. (*C*) Heat capacity for phases I and II, plotted on a log–log scale. Both phases exhibit a T^3 scaling of heat capacity at low temperatures, consistent with a linearly dispersing excitation in 3D. (*D*) Heat capacity of phases N_1 and N_2, plotted on a log–log scale. Both phases exhibit a T^2 scaling of heat capacity at low temperatures, consistent with a linearly dispersing excitation in 2D. This form of dimensional reduction is expected for weakly coupled 2D SNs. (*E*) Heat capacity of magnetization plateau P, showing activated behavior at low temperatures, consistent with the opening of a gap $\Delta = 6.7$ K at 30.2 T.

for the phase N_2, are incompatible with any conventional form of magnetic order (20, 21). The thermodynamic measurements reported in this manuscript supply the missing pieces of this puzzle.

The first crucial piece of evidence comes from the field dependence of the excitation gap with the 1/3-magnetization plateau, P. From measurements of heat capacity, we can identify the lowest-lying excitation within P as a two-magnon bound state, with gap which tends to zero approaching the transition into the phase N_2 (Fig. 4*E*). This result explicitly links the mechanism identified in theory—the condensation of two-magnon bound states (9, 19)—to the phase transition observed in experiment, at low temperatures, as a function of magnetic field.

The second crucial result is clear evidence for a thermodynamic phase transition into the phase N_2, at finite temperature and fixed magnetic field (Fig. 4*B*). This phase transition, which separates the high-temperature paramagnet from a low-temperature, broken-symmetry state, appears to be continuous, with a vanishingly small critical exponent, as found for, e.g., 3D-XY or 2D-Ising universality classes. [We note that an Ising transition is expected for an SN in the presence of Dzyaloshinskii–Moriya interactions (8).]

The third distinct piece of evidence comes from measurements of heat capacity at low temperatures for fixed magnetic field, within the phase N_2. The power-law behavior of heat capacity at low temperature provides clear evidence for the emergence of a Goldstone mode, associated with the breaking of spin rotation symmetry within phase N_2 (Fig. 4*D*). Under other circumstances, such a Goldstone mode could be explained by conventional magnetic order. However, this is ruled out by published NMR results (20, 24), which fail to find the internal field associated with conventional magnetic order within the phase N_2. Taken together, these results make a strong case for SN order, which possesses a linearly dispersing Goldstone mode but does not break time reversal symmetry and so produces no internal field.

Our thermodynamic measurements also clearly identify a second new phase N_1, which is distinct in its properties from N_2. The nature of this phase remains an open question, and at this point it is only possible to speculate as to its origin. The phase N_1 shares a number of features with N_2, including a sharp singularity in heat capacity at the ordering temperature and a T^2 behavior at low T. However, the NMR spectra of phase N_1 contain multiple peaks, which is different from the single-peak feature in N_2, indicating the presence of an internal field in N_1 (20, 24). One possible explanation for this would be a heterogeneity in the crystal (24), but this seems hard to reconcile with the sharpness of the phase transition or the single peak found in phase N_2. An intriguing alternative is the microscopic coexistence of a dipolar SDW and a quadrupolar SN order. It is already known that SDW and SN correlations coexist in the high-field states of frustrated ferromagnetic spin chains (5, 6). Any ordered phase in which both were present would break translational symmetry, through S^z (SDW), making it a solid, and spin-rotation symmetry, through the transverse quadrupole moments Q^{xy} and $Q^{x^2-y^2}$ (SN), making it a superfluid (9, 19). In this sense the phase N_1 could be a supersolid, a state long sought in ^{4}He (28) and also widely discussed in the context of frustrated magnets. The data available for volborthite seem consistent with this interpretation of the phase N_1, but further experimental and theoretical work will be needed to establish its validity.

In summary, in this article we have presented a detailed study of the thermodynamic properties of the frustrated magnetic insulator volborthite, in high magnetic field. These results are summarized in the phase diagram, Fig. 3. We find evidence for the existence of two magnetic phases, labeled N_1 and N_2, at fields approaching the known 1/3-magnetization plateau, P. The thermodynamic properties of the phase N_2, and its previously reported NMR line shape (21), appear to be consistent with the published prediction of SN order (19).

We note that while this article was under review, two studies have also reported the possibility of SN order in the square-lattice frustrated ferromagnet $BaCdVO(PO_4)_2$ (29, 30).

Methods

Materials. Single crystals of volborthite $Cu_3V_2O_7(OH)_2{\cdot}2H_2O$ were grown by the hydrothermal method (31). CuO (99.99%; 6.0 g) and V_2O_5 (99.99%; 3.0 g) powders were mixed in the stoichiometric ratio and were put into a Teflon container together with 1.1 wt % nitric acid (400 mL). Then, the container was placed in a stainless steel vessel and heated to 443 K for 30 d and furnace-cooled to room temperature. Single crystals of volborthite thus obtained are transparent yellow–green, arrowhead shaped, and typically 1 × 0.5 × 0.05 mm in size. They crystallize in the monoclinic *C*2/*c* structure at room temperature. Upon cooling, two structural transitions take place to the *I*2/*m* structure at 290 K and to the $P2_1/a$ structure at 155 K (31). Thus, the

crystal structure of volborthite at low temperatures concerned in the present study is the $P2_1/a$ structure (supplemental material in ref. 20). In this structure, there are two kinds of crystallographically distinguished kagome layers instead of one kind in the $I2/m$ structure. However, the two kagome layers have an identical arrangement of spin-carrying Cu $3d_{x2-y2}$ orbitals and nearly equal bond lengths and angles, suggesting that the magnetic interactions there may be almost the same. In fact, the DFT + U calculations suggest nearly equal magnetic interactions for the two layers (19).

MCE. To determine the *H-T* phase diagram, we performed MCE experiments in a pulsed magnetic field up to 33 T in two different conditions: one is an adiabatic condition (A-MCE), and the other is a nearly isothermal condition (I-MCE).

The field derivative of the isentropic curve $T(H)_S$ obtained by the A-MCE measurement is given by

$$\left(\frac{\partial T}{\partial H}\right)_S = -\frac{T}{C}\left(\frac{\partial M}{\partial T}\right)_H,$$

where S, M, and C are entropy, magnetization, and heat capacity, respectively (22). Thus, the $T(H)_S$ curve is sensitive to any magnetic phase transition. This has been demonstrated for $Sr_3Ru_2O_7$ (32), where multiple kinks in the $T(H)_S$ curves are observed and successfully attributed to a series of field-induced phase transitions.

To decide a phase boundary at lower temperatures, we carried out I-MCE measurements in the nearly isothermal condition. Compared with A-MCE, I-MCE is less sensitive to phase boundaries but can be performed at lower temperatures. Moreover, it yields the field dependence of entropy at an almost constant temperature (32). The I-MCE data are converted to entropy change $\Delta S(H)$ by the equation $\Delta S = \int \kappa(T - T_b)/T dt$, where κ is the thermal conductance between the sample and the surrounding thermal bath and T_b is the temperature of the thermal bath. Assuming a constant value of κ, the field dependence of ΔS is estimated in the arbitrary unit and plotted in Fig. 3*C*.

Heat Capacity Measurements at Flat-Top Pulsed Magnetic Fields. Heat capacity measurements under high magnetic fields above 20 T are not possible in commercial equipment. Either static fields using a big facility or pulsed fields with short time duration are necessary to generate larger magnetic fields. We have employed the latter, but measuring heat capacity in a quickly varying field is challenging. We recently succeeded in developing an experimental technique that allows us to generate a flat-top pulsed magnetic field up to 60 T with the high field stability of ±0.005–0.01 T.

Our strategy for generating a stabilized pulsed magnetic field is depicted in *SI Appendix*, Fig. S1. To generate a time-dependent field of a round arch profile with the top over 40 T, a large current pulse (~10 kA) from the 210-MJ flywheel motor generator is supplied to the main magnet. Slightly before the magnetic field reaches the maximum value, an additional small current (several hundred amperes) from the 50-V lead-acid battery is supplied to a minimagnet set inside the main magnet. When the magnetic field reaches a target value, the field-programmable gate array device starts a PID control of magnetic field for every 2.5 μs. The current flow through the minimagnet (i.e., the magnetic field generated by the minimagnet) is regulated by the resistance of an insulated gate bipolar transistor as commonly used nowadays for motor control in electric cars, trams, and trains. During the PID feedback control, the total field strength was kept at a constant value within ±0.01 T (*SI Appendix*, Fig. S2), and the temperature fluctuation was suppressed at least within ±0.01 K. Within this temperature fluctuation, we could observe a clear temperature increase (ΔT) by the application of a heat (ΔQ) and obtained heat capacity ($C = \Delta Q/\Delta T$) as seen in *SI Appendix*, Figs. S3 and S4. By measuring a Ge polycrystalline sample, we estimated the sensitivity of the present setup in high magnetic field of 43.5 T (*SI Appendix*, Fig. S5).

A series of heat capacity measurements were performed by the quasi-adiabatic method at each flat-top field with time duration of ~0.2 s. A temperature increase ΔT from a starting temperature T_0 after a heat pulse with ΔQ was measured, which yields C as $\Delta Q/\Delta T$. In one shot, more than 10 points of data with varying T_0 were measured, and three to eight pulses were used to get one set of temperature-dependent $C(T)$ data shown in Fig. 4 at each field. We have applied this state-of-the-art technique to study the SN phase of volborthite and obtained a complete *H-T* phase diagram. Detailed explanations on the heat capacity measurements can be found in *SI Appendix*.

ACKNOWLEDGMENTS. We acknowledge fruitful discussions with Tsutomu Momoi, Oleg A. Starykh, Makoto Yoshida, and Masashi Takigawa. We also thank Koushi Kawaguchi and Tadao Imai for their generous help during experiments. This work was supported by Japan Society for the Promotion of Science (JSPS) Grant-in-Aid for Scientific Research (B) Grant 18H01163, by the Core-to-Core Program for Advanced Research Networks given by JSPS, and by the Theory of Quantum Matter Unit of the Okinawa Institute of Science and Technology Graduate University.

1. Andreev AF, Grishchuk IA (1984) Spin nematics. *J Exp Theor Phys* 97:467–475.
2. Blume M, Hsieh YY (1969) Biquadratic exchange and quadrupolar ordering. *J Appl Phys* 40:1249.
3. Mila F (2017) Closing in on a magnetic analog of liquid crystals. *Physics* 10:64.
4. Chubukov AV (1991) Chiral, nematic, and dimer states in quantum spin chains. *Phys Rev B* 44:4693–4696.
5. Hikihara T, Kecke L, Momoi T, Furusaki A (2008) Vector chiral and multipolar orders in the spin-1/2 frustrated ferromagnetic chain in magnetic field. *Phys Rev B* 78:144404.
6. Sudan J, Lüscher A, Läuchli AM (2009) Emergent multipolar spin correlations in a fluctuating spiral: The frustrated ferromagnetic spin-1/2 Heisenberg chain in a magnetic field. *Phys Rev B* 80:140402.
7. Zhitomirsky ME, Tsunetsugu H (2010) Magnon pairing in quantum spin nematic. *Europhys Lett* 92:37001.
8. Starykh OA, Balents L (2014) Excitations and quasi-one-dimensionality in field-induced nematic and spin density wave states. *Phys Rev B* 89:104407.
9. Shannon N, Momoi T, Sindzingre P (2006) Nematic order in square lattice frustrated ferromagnets. *Phys Rev Lett* 96:027213.
10. Ueda HT, Totsuka K (2009) Magnon Bose-Einstein condensation and various phases of three-dimensional quantum helimagnets under high magnetic field. *Phys Rev B* 80: 014417.
11. Shindou R, Yunoki S, Momoi T (2011) Projective studies of spin nematics in a quantum frustrated ferromagnet. *Phys Rev B* 84:134414.
12. Smerald A, Shannon N (2013) Theory of spin excitations in a quantum spin-nematic state. *Phys Rev B* 88:184430.
13. Zhitomirsky ME, Tsunetsugu H (2010) Bose-Einstein condensation of bound magnon pairs. *Europhysics News*, 42:1.
14. Giamarchi T, Rüegg C, Tchernyshyov O (2008) Bose-Einstein condensation in magnetic insulators. *Nat Phys* 4:198–204.
15. Svistov LE, et al. (2011) New high magnetic field phase of the frustrated S = 1/2 chain compound $LiCuVO_4$. *JETP Lett* 93:21–25.
16. Orlova A, et al. (2017) Nuclear magnetic resonance signature of the spin-nematic phase in $LiCuVO_4$ at high magnetic fields. *Phys Rev Lett* 118:247201.
17. Nawa K, et al. (2014) $NaCuMoO_4(OH)$ as a candidate frustrated J_1–J_2 chain quantum magnet. *J Phys Soc Jpn* 83:103702.
18. Nath R, Tsirlin AA, Rosner H, Geibel C (2008) Magnetic properties of $BaCdVO(PO_4)_2$: A strongly frustrated spin-1/2 square lattice close to the quantum critical regime. *Phys Rev B* 78:064422.
19. Janson O, et al. (2016) Magnetic behavior of volborthite $Cu_3V_2O_7(OH)_2{\cdot}2H_2O$ determined by coupled trimers rather than frustrated chains. *Phys Rev Lett* 117:037206.
20. Ishikawa H, et al. (2015) One-third magnetization plateau with a preceding novel phase in volborthite. *Phys Rev Lett* 114:227202.
21. Yoshida M, et al. (2017) Spin dynamics in the high-field phases of volborthite. *Phys Rev B* 96:180413.
22. Schmidt B, Thalmeier P, Shannon N (2007) Magnetocaloric effect in the frustrated square lattice J1-J2 model. *Phys Rev B* 76:125113.
23. Mydosh JA, Oppeneer PM (2011) Colloquium: Hidden order, superconductivity, and magnetism: The unsolved case of URu_2Si_2. *Rev Mod Phys* 83:1301–1322.
24. Yoshida H, et al. (2012) Orbital switching in a frustrated magnet. *Nat Commun* 3:860.
25. Smerald A, Ueda HT, Shannon N (2015) Theory of inelastic neutron scattering in a field-induced spin-nematic state. *Phys Rev B* 91:174402.
26. Wolter AUB, et al. (2017) Field induced quantum criticality in the Kitaev system α-$RuCl_3$. *Phys Rev B* 96:041405.
27. Okubo S, et al. (2001) High-field ESR study of kagome-like substance $Cu_3V_2O_7(OH)_2{\cdot}2H_2O$. *Physica B* 294–295:75–78.
28. Leggett AJ (1970) Can a solid be "superfluid"? *Phys Rev Lett* 25:1543–1546.
29. Povarov KY, et al. (2019) Thermodynamics of a frustrated quantum magnet on a square lattice. *Phys Rev B* 99:024413.
30. Skoulatos M, et al. (2019) Putative spin-nematic phase in $BaCdVO(PO_4)_2$. arXiv: 1903.12462.
31. Ishikawa H, et al. (2012) A novel crystal polymorph of volborthite, $Cu_3V_2O_7(OH)_2{\cdot}2H_2O$. *Acta Crystallogr C* 68:i41–i44.
32. Rost AW, Perry RS, Mercure JF, Mackenzie AP, Grigera SA (2009) Entropy landscape of phase formation associated with quantum criticality in $Sr_3Ru_2O_7$. *Science* 325:1360–1363.